Reconfigurable Workspace and Torque Capacity of a Compliant Ankle Rehabilitation Robot (CARR)

Mingming Zhang, Member, IEEE, Jinghui Cao, Guoli Zhu, Qing Miao, Xiangfeng Zeng, Sheng Q. Xie*, Senior Member, IEEE

Abstract— This paper presents the analysis of the workspace and torque capacity of a compliant ankle rehabilitation robot (CARR). The robot has three rotational degrees of freedom (DOFs) redundantly actuated by four compliant actuators. However, it suffers from conflicting workspace and actuation torque due to the use of a parallel mechanism and compliant actuators. To address these issues, also considering physical constraints imposed by human users, the CARR was designed with reconfigurability to make a trade-off between robot workspace and torque capacity for meeting different training requirements. Theoretical analysis indicates that varying kinematic and dynamic performance of the robot can be achieved by reconfiguring the layout of the actuators. Experiments with/without load also demonstrate the validity of the reconfigurable robotic design for practical applications on robot-assisted ankle rehabilitation. Future work will focus on the design aspects of the robot for easy adjustments, and the integration of force-distribution based actuator force control for optimal robot torque performance.

Index Terms—Ankle robot, compliant, reconfigurable, workspace, torque capacity, rehabilitation

I. Introduction

Robot-assisted rehabilitation solutions, as therapeutic adjuncts to facilitate clinical practice, have been actively researched in the past few decades [1]. A systematic review of 29 studies with a total of 164 patients and 24 healthy subjects demonstrates the effectiveness of existing rehabilitation robots in reducing ankle impairments [2]. However, parallel robots are better suited for ankle exercises due to the characteristics of multiple degrees of freedom (DOFs), safe workspace and large actuation torque with respect to wearable exoskeletons that aim at gait exercises [3] and ankle devices with a single DOF [4].

Several robotic platforms have been developed for ankle therapy based on parallel mechanisms. A typical instance is the Rutgers Ankle powered by double-acting pneumatic cylinders [5]. While its effectiveness has been demonstrated on subjects with varying grades of ankle sprains [6], stroke patients [7], and children with cerebral palsy [8], it should be noted that the Rutgers Ankle has difficulties in defining training protocols due to misaligned rotation center as the anatomical ankle joint, or limited workspace unless using longer actuators. Saglia, Tsagarakis [9] also developed a parallel ankle rehabilitation robot using three motor-based linear actuators. While a high-performance interaction controller has been implemented for active exercises [10], the use of a central strut makes the rotation of its moving platform misaligned with the ankle joint.

To allow compatible robot structure for ankle rehabilitation, Tsoi, Xie [11] replaced a middle passive link with the lower limb of the patient on a parallel ankle robot. This design can match the anatomical ankle joint by placing four actuators above the end effector (AaEE), but unexpected loads may be exerted causing uncomfort and safety issues. Jamwal, Xie [12], more advanced, constructed a three-DOF robotic device by setting physical rotation axes for the moving platform to reduce direct interaction with the ankle joint. They adopted four pneumatic muscle actuators to achieve the compliance of the ankle device, but this design has the issue of limited actuation torque at maximum muscle contraction. While the robots developed by Tsoi, Xie [11] and Jamwal, Xie [12] have been demonstrated with great potential for ankle rehabilitation due to the use of parallel mechanisms with AaEE, the other way to achieve three DOFs and aligned rotation center has been proposed by Wang, Fang [13]. An obvious advantage of this robotic design is the shallow depth for human lower limbs, but this required extra accessory structure as leg support. However, this design does not allow the robot to be adjusted to an arbitrary angle for adapting varying sitting postures of patients. More significantly, this robot has not been validated experimentally in terms of actuation capacity and clinical applicability.

The robotic training can be passive, active-assist and active range of motion (ROM) exercises, as well as muscle strengthening schemes. Passive ROM exercises involve the robot guiding the patient's ankle through the predefined training trajectory when the patient's foot remains relaxed. Active-assist ROM exercises on the other hand require the robot to cooperate with the patient to perform the predefined motion, providing certain assistance based on real-time ankle assessment. Active ROM exercises are conducted completely depending on the patient's intention and ankle capacity with minimal human-robot interaction. For muscle strength training

This work was supported by the University of Auckland, Faculty of Engineering Research Development Fund 3625057 and the China Sponsorship Council.

M. Zhang, S. Xie (Corresponding author), J. Cao, Q. Miao are with the Department of Mechanical Engineering, Auckland University, 20 Symonds Street, Auckland, New Zealand. (e-mail: mzha130@aucklanduni.ac.nz, s.xie@auckland.ac.nz, jcao027@aucklanduni.ac.nz, miaoqing0702@126.com).

G. Zhu is with the Department of Mechanical Engineering at Huazhong University of Science and Technology, 1037 Luoyu Road, Wuhan, Hubei, China (e-mail: glzhu@mail.hust.edu.cn, allen_zengzz@hotmail.com).

exercises, the robot should be able to provide certain resistance to the foot according to the joint position and capacity to challenge the patient over time. Hence different rehabilitation modes require different robot workspace and actuation torque. A suitable robot workspace and actuation torque can also enhance the training safety.

Taking all into consideration, an ideal rehabilitation robot for comprehensive ankle therapy should have intrinsic compliance, suitable workspace and torque actuation capacity, aligned rotation center with ankle joint, and adjustable structure for using on different sitting postures of patients. Zhang [14] has developed a novel compliant ankle rehabilitation robot (CARR). While this robot was designed with reconfigurable structure aiming to achieve varying workspace and actuation torque, the theoretical analysis and experimental validation have not yet been conducted.

It is also well known that the limited workspace of parallel manipulators, in comparison to serial ones, is a drawback, which conversely can be an advantage for rehabilitation purpose due to training safety. The use of pneumatic muscle actuators also makes the torque capacity of the robot very limited at maximum muscle contraction. Therefore, there must be some tradeoffs between robot workspace and torque capacity depending on a specific training protocol for an individual, and optimization techniques should be involved to ensure the kinematic and dynamic performance of the CARR with various configurations. To the best of the authors' knowledge, this is a first ever attempt, in the field of parallel mechanisms, wherein a multi-DOF ankle rehabilitation robot can be reconfigured to achieve varying workspace and torque actuation capacity. This paper is organized in the order of introduction, robot design, analysis on robot workspace and torque capacity, experimental results, discussion and conclusion.

II. Reconfigurable Robot Design

The three-dimensional model of the CARR is presented in Fig. 1. It consists of a fixed platform and a moving one which are connected together with four compliant actuators (spherical-prismatic-spherical). Thus the kinematic structure of the robot has four closed kinematic pairs and the motions are achieved through simultaneous motion of these four kinematic pairs. Four Festo fluidic muscles (FFMs) are selected for comfort and safety, also with high actuation force. This robot has three rotational DOFs that are for ankle dorsiflexion/plantarflexion (DP), inversion/eversion (IE), and adduction/abduction (AA), respectively. The number of robot DOFs is calculated using the Chebyshev-Grubler-Kutzbach criterion [15]. That is, $F = \lambda(n-j-1)+\sum_{i=1}^{j} f_i - f_p$, F refers to the DOFs of the mechanism, λ refers to the DOFs of the space, n is the number of all links including the base, j is the number of binary joints, f_i is the DOFs permitted by joint i, and f_p is denoted for the total number of passive DOFs.

As described in Fig. 1, the fixed platform consists of an upper fixed platform (UFP) and a lower fixed platform (LFP), while the moving platform (MP) is actually a three-linkage serial mechanism with three rotational DOFs. The third link of the MP is also the end effector. The MP is connected with the LFP by a revolute pair. The rotation axes of ankle DP, IE and AA are denoted as X_m, Y_m, and Z_m, respectively.

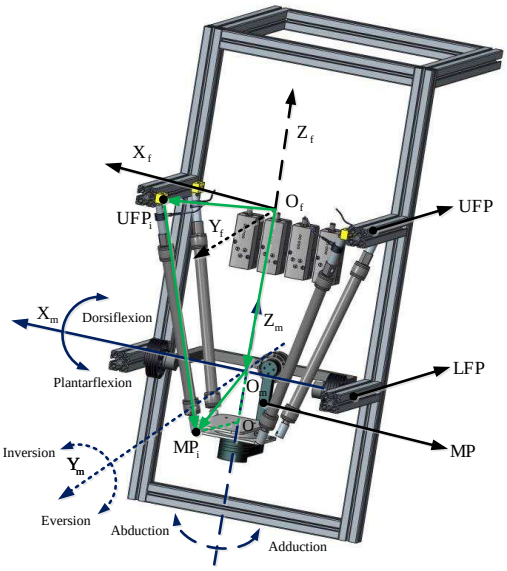

Fig. 1. Geometrical description of the CARR mechanism and motions.

A. Robot Kinematics and Dynamics

The line sketch of the ith actuator is presented in Fig. 1 in an initial state, and the coordinate of its connection point is shown in Fig. 2. The fixed coordinate system is denoted as $O_f X_f Y_f Z_f$ and the moving coordinate system is denoted as $O_m X_m Y_m Z_m$ Connection points of the ith actuator on the UFP and the MP are denoted as UFP_i and MP_i, respectively. Their position vectors P_i^f and P_i^m are defined in (1), as well as the relative position vector O of two coordinate systems, where H refers to the distance between the origins of the UFP and the LFP, h is the distance from O_m to O_e.

$$\begin{cases} P_i^f = \overrightarrow{O_f UFP_i} = [x_i^f \quad y_i^f \quad 0]^T \\ P_i^m = \overrightarrow{O_m MP_i} = [x_i^m \quad y_i^m \quad -h]^T \qquad i = 1,\dots,4. \\ O = \overrightarrow{O_f O_m} = [0 \quad 0 \quad -H]^T \end{cases} \tag{1}$$

Position vectors of the actuators can be expressed as a system of four equations in terms of the posture of the end effector, denoted as L_i^f in (2-4). The transformation matrix R_m^f of the moving platform with respect to the fixed one is defined in (3) and (4) using a fixed axis rotation sequence of its orientation θ_x, θ_y and θ_z. The Jacobian matrix of this robot design maps the Cartesian velocities to the actuator velocities. It is derived in (5) and (6), where l_i^f refers to the length of the ith actuator as $\sqrt{(L_i^f)^T L_i^f}$.

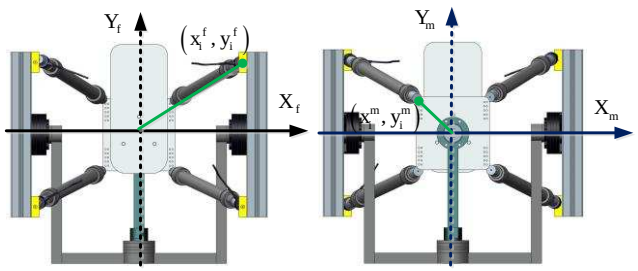

Fig. 2. The definition of connection points of each actuators.

$$L_i^f = O + R_m^f P_i^m - P_i^f \qquad i = 1, \dots, 4. \tag{2}$$

$$R_m^f = \begin{bmatrix} cos\theta_z cos\theta_y & R_{12} & R_{13} \\ sin\theta_z cos\theta_y & R_{22} & R_{23} \\ -sin\theta_y & cos\theta_y sin\theta_x & cos\theta_y cos\theta_x \end{bmatrix} \tag{3}$$

$$\begin{cases} R_{12} = -sin\theta_z cos\theta_x + cos\theta_z sin\theta_y sin\theta_x \\ R_{13} = sin\theta_z sin\theta_x + cos\theta_z sin\theta_y cos\theta_x \\ R_{22} = cos\theta_z cos\theta_x + sin\theta_z sin\theta_y sin\theta_x \\ R_{23} = -cos\theta_z sin\theta_x + sin\theta_z sin\theta_y cos\theta_x \end{cases} \tag{4}$$

$$J = [J_1,\ J_2,\ J_3,\ J_4]^T \tag{5}$$

$$J_i = \left[P_i^f \times \frac{L_i^f}{l_i^f} \right]^T \qquad i = 1, \dots, 4. \tag{6}$$

The condition number of the Jacobian matrix, a measure of robot singularity, provides a relation between changes in the joint space and task space kinematic variables. Thus, the geometrical parameters of the CARR have to been carefully selected to avoid the robot configuration becoming singular. The condition number is an important robot design parameter and solely depends on the physical construction of a robot. It has important physical significance. A robot design with near unity condition number is desirable [16] since it minimizes the error of the torque of the robot end effector. The condition number can also be used to evaluate the workspace singularities. It reveals how far the robot is from its present configuration to the nearest singular configuration.

Though the Jacobian matrix is not a square matrix for the CARR, its singular values σ_i can be still calculated in (7),

$$\sigma_i = \sqrt{\lambda_i (J^T J)} \tag{7}$$

where λ_i is the eigenvalue of the matrix $J^T J$. The condition number k can be given in (8), where σ_{max} and σ_{min} are the maximum and minimum singular values of the matrix J, respectively.

$$1 \le k = \frac{\sigma_{max}}{\sigma_{min}} \le \infty \tag{8}$$

To evaluate the robot design, the condition number is generally obtained at different workspace points on the specified robot trajectory with assumed resolution. Though the condition numbers k_i at different end effector orientations are useful, to get a comprehensive view of its distribution in the entire workspace volume, a Global Condition Number (GCN) given in (9) is normally used [17].

$$GCN = \frac{\sum_{i=1}^{n} (k_i)}{n} \tag{9}$$

Here n is the total number of discrete feasible points constituting the workspace and the numerator is the sum of condition numbers obtained at these points in the feasible workspace volume grid. The global condition number is bounded by the range as given in (10).

$$1 \le Global\ Condition\ Number\ (GCN) \le \infty \tag{10}$$

The exerted torque in task space can be obtained using (11) based on individual actuator force. In return, the required individual actuation force can be calculated in (12) for a given task space torque, where $\bar{J} = J(J^T J)^{-1}$ is the pseudo inverse of the matrix J^T. Cable-driven robots may lose controllability if certain cables are not in tension during the robotic operation [18]. Thus optimization based techniques should be involved on the CARR to ensure all FFMs in tension for training safety, but with minimum force values for larger workspace. An analytic-iterative force distribution method proposed by Taghirad et al. [19] can be used to control the forces of stretched actuators at predefined positive values for minimum energy consumption and training safety, by which the CARR can achieve larger workspace.

$$T_{3\times 1} = J^T [F_1,\ F_2,\ F_3,\ F_4]^T \tag{11}$$

$$F_{4\times 1} = \bar{J} \left[T_x,\ T_y,\ T_z \right]^T \tag{12}$$

B. Robot Reconfigurability

Robot-assisted rehabilitation strategies can be ROM or muscle strengthening exercises. ROM exercises require the robot have a larger workspace than actual ankle motions, while muscle strengthening exercises require it have high actuation torque. Due to the use of pneumatic actuators, the CARR has quite limited torque capacity at maximum FFM contraction where the maximum workspace is achieved. Specifically, there must be some tradeoffs between the robot workspace and torque actuation capacity. Thus, the CARR has to be designed with reconfigurability in providing adjustable workspace and actuation torque for a variety of training strategies, as described in Fig.3. A reconfigurable architecture of the CARR consists of a set of configurations by selecting different numbers and types of modules, and setting different combinations of mounting dimensions.

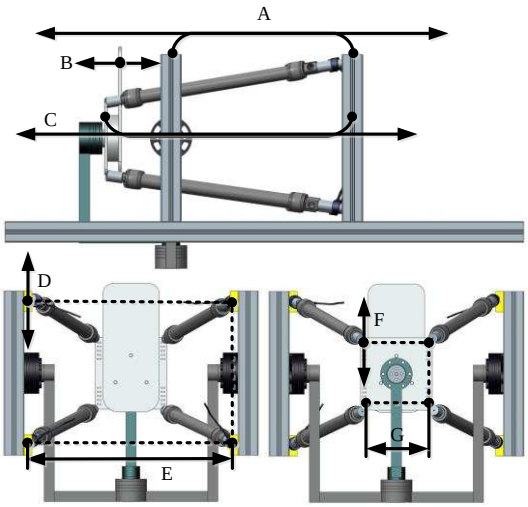

Fig. 3. Reconfigurability of the CARR. The arrow represents the adjustment direction, black points connected by dash dot lines have adjustment in the same direction. (A: the adjustment of the fixed platform along the sliding rail for different sizes of patients' lower limbs; B: the adjustment of the footplate for different sizes of patients' feet; adjustments A and B do not affect the robot workspace and actuation torque; C: the adjustment of the end effector and the UFP, which can change the distance of the footplate and the UFP; D: the y-direction adjustment of connection points of the actuators on the UFP; E: the x-direction adjustment of connection points of the actuators on the UFP; F: the y-direction adjustment of connection points of the actuators on the end effector; G: the x-direction adjustment of connection points of the actuators on the end effector; adjustments C, D, E, F, G all affect the robot workspace and actuation torque).

C. Actuator Modeling

FFMs can generate a larger force with the same size and contraction length compared to traditional pneumatic actuators, which makes them increasingly popular in robotic rehabilitation devices. Robot-assisted ankle rehabilitation exercises are considered to be slow and in quasi-static environment. Therefore, the function approximation proposed by Sarosi [20] is adopted in this study to derive the FFM contraction force based on its pressure and contraction strain, as in (13), where the muscle contraction strain $s = \frac{l_0 - l}{l_0}$, and the pulling force F, the applied pressure p, l_0 and l respectively represent the initial muscle length and the actual length. Parameters a, b, c, d, e are arbitrary coefficients that were experimentally obtained by fitting the model to the data by changing the muscle length when the tensile force and pressure were recorded. For inflation of the FFM (DMSP-20-400-RM-RM), a=232.89, b=-38.32, c=-904.01, d=294.86 and e=-289.06, while for deflation a=272.70, b=-32.58, c=-908.24, d=298.83 and e=-262.85.

$$F(p,s) = (p + a)e^{bs} + cps + dp + e \tag{13}$$

III. Adjustable Workspace and Actuation Torque

A. Ankle Motion and Torque

Three-dimensional ankle ROMs suggested by Siegler, Chen [21] will be considered as references for designing the CARR, as summarized in Table 1. It can be seen that ankle ROMs in different directions are quite different, with around -45° to 25° for DP, -15° to 20° for IE, and -20° to 25° for AA. Torque capacity has to be also considered in designing the robot, especially for muscle strengthening exercises. The maximum passive ankle torques obtained by Parenteau, Viano [22] from 32 human lower legs are also summarized in Table 1.

Table 1. Typical ROMs [21] and passive torque [22] of the human ankles.

Type of motion	Ankle Motions			Maximum PAT (Nm)
	ROM	Mean	SD	
Dorsiflexion	20.3° to 29.8°	24.68°	3.25°	34.1±14.5
Plantarflexion	37.6° to 45.75°	40.92°	4.32°	48.1±12.2
Inversion	14.5° to 22°	16.29°	3.88°	33.1±16.5
Eversion	10° to 17°	15.87°	4.45°	40.1±9.2
Adduction	22° to 36°	29.83°	7.56°	NA
Abduction	15.4° to 25.9°	22.03°	5.99°	NA

PAT: Passive ankle torque; SD: Standard deviation; NA: Not available.

B. Condition Number

The condition number will be used to analyze singularity of the CARR. The joint-space actuator forces cannot provide effective actuation torque in the task space of the robot at a singular configuration, so it is imperative to eliminate singularity in actual robot workspace. The CARR has been developed in Mechatronics Lab of the University of Auckland by our group [14]. Although this robot can achieve adjustable workspace and actuation torque based on adjustments presented in Fig. 3, its kinematic and dynamic performance has not been evaluated. The default configuration of the CARR is presented in Table 2, where only parameters affecting robot workspace and torque capacity are given.

Table 2. The kinematic configuration of the CARR.

Robot configuration	Absolute values of coordinates	
	X	Y
Distance between UFP and LFP (Adjustment C)	445 mm	
Connection points of FFMs on the UFP (Adjustments D and E)	202.5 mm	140 mm
Connection points of FFMs on the LFP (Adjustments F and G)	65 mm	60 mm

UFP: Upper fixed platform; LFP: Lower fixed platform.

The CARR can operate with three rotational DOFs (ankle DP, IE and AA) or two DOFs (ankle DP and IE) depending on specific rehabilitation strategies. For these cases, the condition numbers of the robot present significantly different, as presented in Figs. 4 and 5. When the robot operates with three DOFs, the GCN is 11.18 in Fig. 4 for a predefined robot workspace, ranging from -46° to 46° respectively about axes X_m, Y_m, and Z_m. In fact, the actual ankle workspace can be smaller with respect to this predefined one, which means that the real GCN is less than 11.18 for actual robot workspace of ankle training. However, these configurations were only preliminarily selected and further optimization should be involved to enhance the kinematic and dynamic performance. Jamwal, Hussain [23] proposed a three-stage analysis techniques, including kinematic design, actuation design, and structural design, to solve the issues in the pretext of a parallel mechanism designed for ankle therapy. This analysis method can be used for the optimization of the CARR with minor adaptations. Depending on a specific training strategy, the CARR can be reconfigured into a two-DOF mechanism by

locking the motion of robot AA, where a better kinematic and dynamic performance can be achieved with the GCN being 1.24 in Fig. 5. It should be noted that the Z in Fig. 4 is a variable while that of Fig .5 represents some discrete constants depending on the locking positions. Throughout this paper, the X, Y and Z values in all Figs refer to the angular positons about axes X_m, Y_m, and Z_m, respectively.

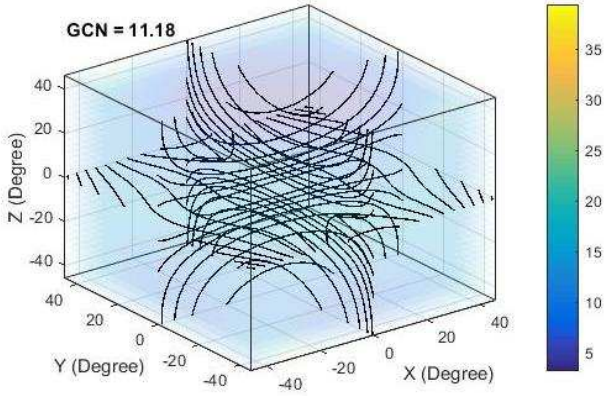

Fig. 4. Condition number of the CARR with three DOFs (ankle DP, IE and AA).

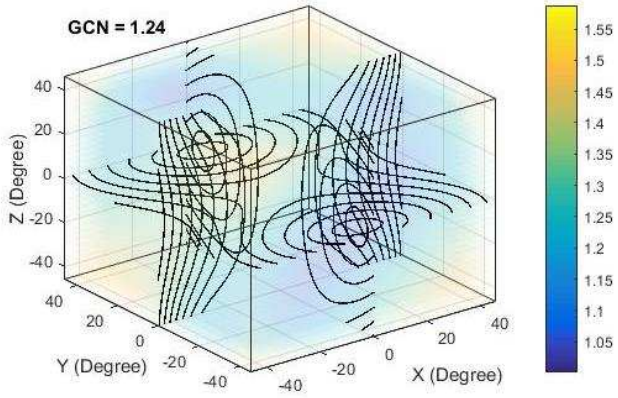

Fig. 5. Condition number of the CARR with two DOFs (ankle DP and IE).

C. Robot Workspace

A compact design requires that the used actuator should have a short length to keep the total depth of the robot close to the size of the patient's shinbone. Inverse kinematics is used to calculate the displacements of the actuators for a given robot workspace. When one of the displacement values exceeds the stroke of the actuator, this pose is unreachable and will be excluded, as in (14). The interference between actuators and human lower limbs should be also avoided for smooth motion control and training safety, although the FFM has intrinsic compliance. This constrain is defined in (15), where $\aleph(L_i^f,\ O_m)$ is the function to calcualte the spatial distance between the ankle joint O_m and the ith actuator L_i^f, and $\complement$ is a constant depending on the patient's ankle size. In addition, to guarantee the to-and-fro motion control of the CARR, the connection point $\beth(R_m^f P_i^m)$ of the ith actuator on the MP should fall inside the ith quadrant Q_i of the $X_m - Y_m$ plane, as in (16).

$$-0.02 \le s = \frac{l_0 - l}{l_0} \le 0.28 \tag{14}$$

$$\aleph(L_i^f,\ O_m) \ge \complement \tag{15}$$

$$\beth(R_m^f P_i^m) \in Q_i \tag{16}$$

By examining each point in the predefined workspace based on the three constrains (14-16) under the default configuration presented in Table 2, the effective robot workspace is obtained in Fig. 6. This configuration allows for a three-dimensional workspace, ranging from -35.5° to 35.5° for ankle DP, -34.4° to 34.4° for IE, and -45.9° to 45.9° for AA. Comparing with the data presented in Table 1, the robot ROMs of ankle IE and AA are obviously larger than actual ankle motions. For ankle training in the sagittal plane, the maximum achieved dorsiflexion of the CARR can also meet the requirement of most cases, such as the treatment of ankle stretching of drop foot, while the maximum plantarflexion is less than actual ankle motion.

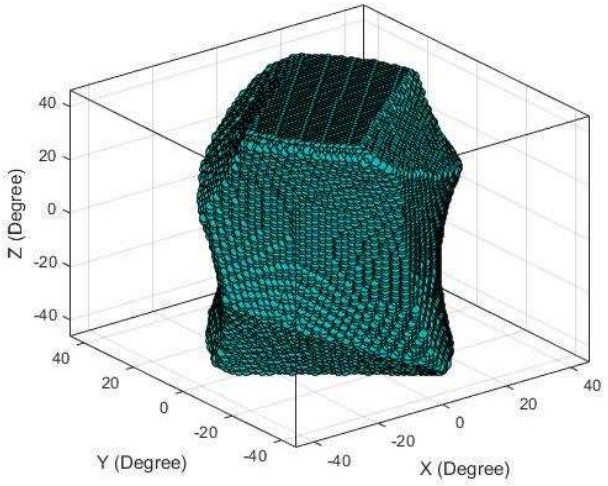

Fig. 6. Workspace of the CARR in a three-dimensional space. (X_Min = -35.5°, and X_Max = 35.5°; Y_Min = -34.4 °, and Y_Max = 34.4°; and Z_Min = -45.9°, and Z_Max = 45.9°)

Since the CARR was designed with reconfigurability in achieving adjustable workspace, we made the adjustment F for instance, with the absolute values of the y-coordinate of all connection point of actuators on the MP changed from 60mm to 44mm. Under this new configuration, the effective robot workspace has been also adjusted and presented in Fig. 7, where the green dot represents the data of Fig. 6 and blue dots refer to new added workspace. It can be seen that the robot ROM for ankle plantarflexion has been slightly increased from -35.5° to -36.7°. While the robot ROM for ankle IE is reduced, it still meet the requirement of ankle therapy in the frontal plane.

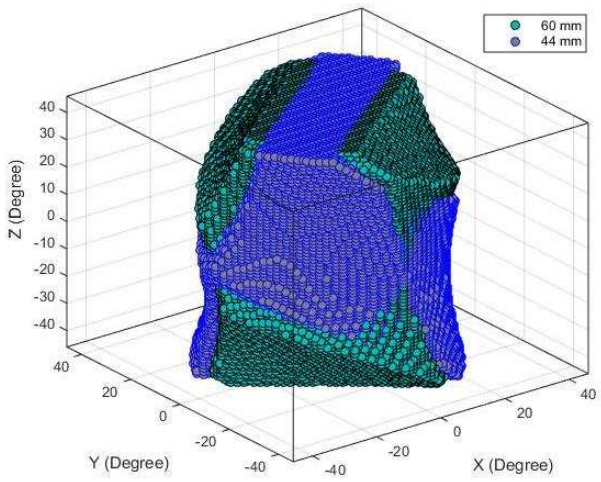

Fig. 7. Workspace of the CARR in a three-dimensional space. (X_Min = -36.7°, and X_Max = 36.7°; Y_Min = -33.2 °, and Y_Max = 33.2°; and Z_Min = -45.9°, and Z_Max = 45.9°)

D. Robot Torque Capacity

For a given pose of the end effector, individual FFM length can be calculated by inverse kinematics (2-4). The contraction force of the actuator can be obtained using (13) by transforming the muscle length to strain. Hence the robot torque $T_{3\times1}$ can be given in (11). The overall stiffness matrix of the CARR, from its actuator stiffness, is computed using (17-19), where K is the robot stiffness, F is the contraction force of the FFM, and k_i is the stiffness of the ith actuator.

$$K = J^T S J \tag{17}$$

$$S = \frac{dF}{dl} = diag(k_1, k_2, k_3, k_4) \tag{18}$$

$$k_i = -\frac{b(p+a)}{l_0} e^{b\left(1-\frac{l}{l_0}\right)} - \frac{lp}{l_0} \quad i = 1, \dots, 4. \tag{19}$$

Taking the same adjustment F from 60 mm to 44 mm as in previous subsection, the torque capacity of the CARR is derived using (11). As in Fig. 8, the top plot represents the robot torque for ankle DP, the middle one plots the robot torque for ankle IE and the bottom one is the torque for ankle AA. It is clear that the torque capacity of the CARR for ankle IE and AA under default configuration presents small changes after adjustment, while the robot torque for ankle DP presents significant changes due to the decrease of force arm of the actuators. As shown in the top plot of Fig. 8, the torque capacity of the robot is large enough for a variety of ankle exercises in most range of ankle DP. However, the robot torque becomes close to zero at around -35° of ankle plantarflexion, which may lead to insufficient robot torque for further ankle stretching, and thus optimization techniques should be involved to address this issue.

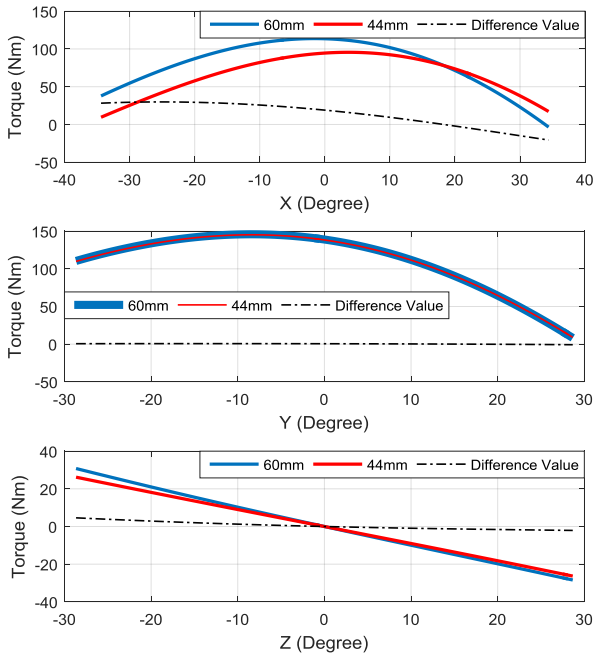

Fig. 8. Torque capacity of the CARR under the adjustment F from 60 mm to 44 mm.

IV. Experimental Results

While theoretical analysis has suggested the ability of the CARR in achieving adjustable robot workspace and actuation torque, experiments were still conducted to validate the reconfigurability of the robot. A healthy subject (male, 31 years, height: 172 cm and weight: 75 kg) participated in this study. He gave written consent to participate in the trial according to ethics approval obtained from the University of Auckland, Human Participants Ethics Committee (011904).

All desired trajectories take the form of sinewave with frequency being 0.05 Hz. Experiments were firstly conducted on the CARR without any load with the default configuration. The predefined amplitude of the sinewave is 31.5°, while the actual achieved ROM for ankle DP is from -29.48° to 28.51°, as shown in the top plot of Fig. 9. This is the maximum achieved ROM of the robot for ankle DP since the predefined value is not reached. For trajectory tracking of ankle IE, the achieved ROM compares well with the predefined value 17.2°. Experiments were then conducted with the participant on load with the same desired amplitude. It is presented in the top plot of Fig. 9 that the achieved ROM of ankle DP ranges from -28.07° and 25.61°. The corresponding ankle torques about axes-X, -Y are plotted in the middle of Fig. 9. By comparison, the achieved ROM of ankle DP with load is less than that of without load, and the possible reason can be insufficient actuation torque at extreme ROM.

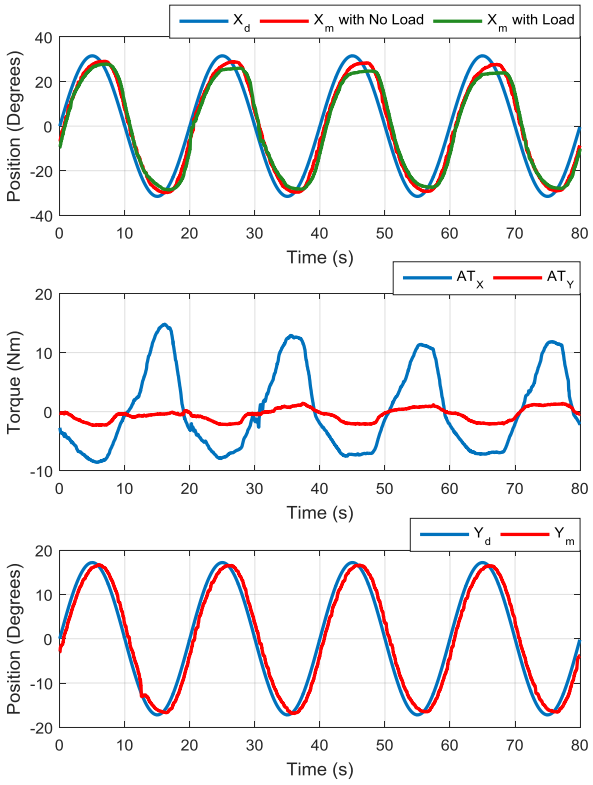

Fig. 9. ROMs of the CARR with the configuration (X65Y60). (Averaged plantarflexion and dorsiflexion through four cycles with no load being -29.48° and 28.51°, respectively; the values with the participant are -28.07° and 25.61°, respectively)

After reconfiguration of the CARR with the same adjustment from 60 mm to 44 mm, the same experiments were conducted with/without load, respectively. The predefined amplitude was changed to 37.3°, and the actual achieved ROM for ankle DP is from -35.52° and 33.71°, as shown in the top plot of Fig. 10. In the same way, this is also the maximum achieved ROM of the robot for ankle DP. The trajectory tracking of ankle IE can still reach the predefined value 17.2°. Experiments were finally conducted with the participant. The top plot of Fig. 10 shows that the achieved ROM of ankle DP ranges from -35.18° and 31.35°. The corresponding ankle torques are presented in the middle of Fig. 10. Comparison shows that the achieved ROM of ankle DP with load is also less than that of without load, and the possible reason can also be insufficient actuation torque at extreme ROM. However, by comparing the performance of the robot reconfiguration in Figs. 9 and 10, the ankle DP ROM is increased by reducing the force arm of the actuator, while the robot ROM for ankle IE in both configurations can meet the requirement of therapy training.

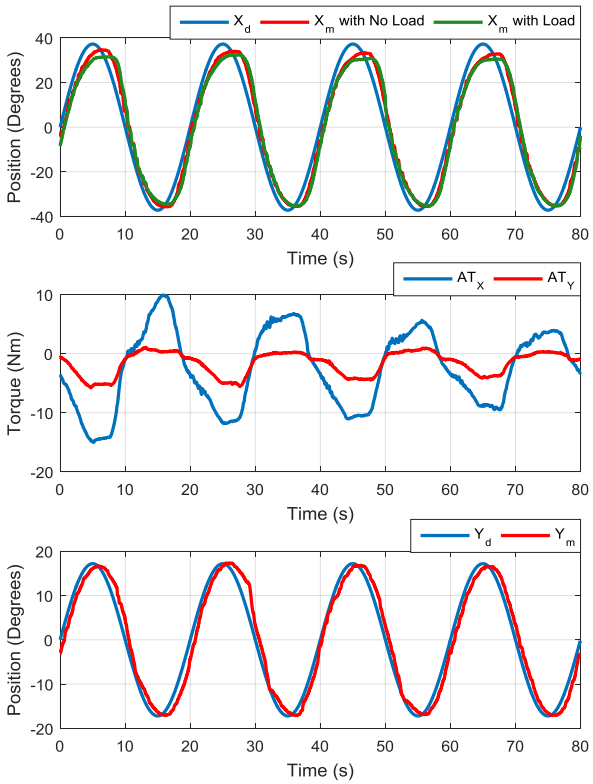

Fig. 10. ROMs of the CARR with the configuration (X65Y44). (Averaged plantarflexion and dorsiflexion through four cycles with no load being -35.52° and 33.71°, respectively; the values with the participant are -35.18° and 31.35°, respectively)

V. Discussion and Conclusion

This paper presents the analysis of the workspace and torque capacity of the CARR. Since this robot is based on a parallel mechanism with three rotational DOFs redundantly actuated by four compliant FFMs, some conflicts exist including workspace and actuation torque. Hence this robot designed with enough workspace and actuation torque is hard to be achieved unless the use of longer FFMs. It should be noted that longer FFMs are not desired on an ankle rehabilitation robot for adapting different sizes of human shanks.

An optimal robot for ankle rehabilitation should be able to deliver subject-specific training exercises with appropriate workspace and torque capacity. While the use of compliant FFMs can make robot-assisted ankle training comfortable and safe, an issue is the limited actuation torque at extreme robot workspace, as demonstrated in Figs 8, 9 and 10. The robot with suitable workspace and actuation torque can also ensure the training safety. The CARR developed by Zhang [14] was designed with reconfigurability in achieving adjustable robot workspace and actuation torque, which has been demonstrated as an excellent solution to ankle rehabilitation robots with conflicted workspace and actuation torque. Based on assessment of ankle motions and torque capacity of the patients, the CARR can be reconfigured with appropriate workspace and actuation torque indexes for a specific training strategy.

Again refers to the bottom plot of Fig. 8, the actuation torque of the robot is close to zero at 0° of ankle AA, which makes the

passive streching ankle exercises impossible. The reason can be the symmetrical layout of the actuators, and optimization based techniques have been well used to address this issue [12, 24, 25]. However, how much the robot torque can be improved is not clear and should be further investigated for clinical applications. A more direct method is to use a motor instead for actuating ankle AA. This novel mechanism with hybrid power can not just make the control along ankle AA easier, but also improve the kinematic performance of the CARR, as demonstated in Figs. 4 and 5 where a better kinematic and dynamic performance is achieved with the GCN being 1.24 with only ankle DP and IE.

As Qian and Bi [26] suggested, main obstacles of the promotion of rehabilitation robots in real life are the lacking of personalization and excellent cost performance. Hence using a reconfigurable and modular architecture can be a good method to make a trade-off for this conflict. The CARR design with reconfigurability can definitely promote its application due to more functionalities and thus target more patients. A more direct comparison with the reconfigurable CARR is another ankle robot developed by Yoon and Ryu [27]. That device can be used for ROM and muscle strengthening exercises, as well as the balance and proprioception training by adding an extra large plate. An obvious difference of these two reconfigurable ankle robots is that the CARR can generate adjustable workspace and actuation torque, while the robot by Yoon and Ryu [27] was designed for more functions.

Theoretical computation has demonstrated the ability of the CARR in achieving adjustable workspace and actuation torque. Experiments also support its validity for practical applications. However, some limitations exist. Firstly, the calculation of the contraction forces of the FFMs is based on a static model, which can make the estimation of the robot torque capacity inaccurate in a dynamic environment of rehabilitation exercises. Second, in terms of key dimensions, the physical structure of the CARR can be slightly different with the theoretical values used in the simulation due to assembly precision. This could cause some differences between the theoretical robot workspace and the actual achieved one. Third, only adjustment F was made for instance, and comprehensive analysis should be conducted. Last but most significantly, it is assumed in the theoretical analysis that the stretched actuator force was kept a constant positive value to ensure all actuators in tension for training safety and also increase the robot torque. In contrast, the control of the robot prototype was based on the length control of individual actuators without force control involved. However, this does not significantly affect the validation of the robot workspace.

To summarize, this is the first attempt to analyze the workspace and torque capacity of the CARR. Both theoretical analysis and experimental results have demonstrated the ability of the robot in generating varying workspace and actuation torque depending on different configurations. Such a design can be an ideal solution to parallel ankle rehabilitation robots actuated by compliant actuators. Future work will focus on the design aspects of the robot to allow for easy adjustments, and the integration of force-distribution [19] based actuator force control for maximum robot torque capacity.

ACKNOWLEDGMENTS

This material was based on work supported by the University of Auckland, Faculty of Engineering Research Development Fund-3625057 (Physical Robot-Human Interaction for Performance-Based Progressive Robot-Assisted Therapy). The authors have declared that no competing interests exist.

REFERENCES

[1] Krebs HI, Palazzolo JJ, Dipietro L, Ferraro M, Krol J, Rannekleiv K, et al. Rehabilitation robotics: performance-based progressive robot-assisted therapy. Auton Robot. 2003;15:7-20.
[2] Zhang M, Davies TC, Xie S. Effectiveness of robot-assisted therapy on ankle rehabilitation - a systematic review. Journal of NeuroEngineering and Rehabilitation. 2013;10:30.
[3] Roy A, Krebs HI, Williams DJ, Bever CT, Forrester LW, Macko RM, et al. Robot-aided neurorehabilitation: a novel robot for ankle rehabilitation. IEEE Transactions on Robotics. 2009;25:569-82.
[4] Waldman G, Yang CY, Ren Y, Liu L, Guo X, Harvey RL, et al. Effects of robot-guided passive stretching and active movement training of ankle and mobility impairments in stroke. NeuroRehabilitation. 2013;32:625-34.
[5] Girone M, Burdea G, Bouzit M, Popescu V, Deutsch JE. A stewart platform-based system for ankle telerehabilitation. Auton Robot. 2001;10:203-12.
[6] Deutsch JE, Latonio J, Burdea GC, Boian R. Rehabilitation of musculoskeletal injuries using the Rutgers Ankle haptic interface: three case reports. Proceedings of Eurohaptics. Birmingham, UK2001. p. 11-6.
[7] Deutsch JE, Latonio J, Burdea GC, Boian R. Post-stroke rehabilitation with the Rutgers Ankle system: a case study. Presence. 2001;10:416-30.
[8] Cioi D, Kale A, Burdea G, Engsberg J, Janes W, Ross S. Ankle control and strength training for children with cerebral palsy using the Rutgers Ankle CP: a case study. IEEE International Conference on Rehabilitation Robotics. ETH Zurich Science City, Switzerland2011. p. 654-9.
[9] Saglia JA, Tsagarakis NG, Dai JS, Caldwell DG. A high-performance redundantly actuated parallel mechanism for ankle rehabilitation. The International Journal of Robotics Research. 2009;28:1216-27.
[10] Saglia JA, Tsagarakis NG, Dai JS, Caldwell DG. Control strategies for patient-assisted training using the ankle rehabilitation robot (ARBOT). IEEE/ASME Transactions on Mechatronics. 2013;18:1799-808.
[11] Tsoi YH, Xie SQ, Graham AE. Design, modeling and control of an ankle rehabilitation robot. Studies in Computational Intelligence. 2009;177:377-99.
[12] Jamwal PK, Xie SQ, Hussain S, Parsons JG. An adaptive wearable parallel robot for ankle injury treatments. IEEE/ASME Transactions on Mechatronics. 2014;19:64-75.
[13] Wang C, Fang Y, Guo S, Chen Y. Design and Kinematical Performance Analysis of a 3-RUS/RRR Redundantly Actuated Parallel Mechanism for Ankle Rehabilitation. Journal of Mechanisms and Robotics. 2013;5:041003-.
[14] Zhang M. Improving Effectiveness of Robot-Assisted Ankle Rehabilitation via Biomechanical Assessment and

Interaction Control. Auckland, New Zealand: University of Auckland; 2016.
[15] Grübler MF. Getriebelehre: eine Theorie des Zwanglaufes und der ebenen Mechanismen. Berlin: Springer; 1917.
[16] Khatami S, Sassani F. Isotropic design optimization of robotic manipulators using a genetic algorithm method. IEEE International Symposium on Intelligent Control - Proceedings. Vancouver2002. p. 562-7.
[17] Gosselin C, Angeles J. A Global Performance Index for the Kinematic Optimization of Robotic Manipulators. J Mech Design. 1991;113:220-6.
[18] Hassan M, Khajepour A. Analysis of bounded cable tensions in cable-actuated parallel manipulators. IEEE Transactions on Robotics. 2011;27:891-900.
[19] Taghirad HD, Bedoustani YB. An analytic-iterative redundancy resolution scheme for cable-driven redundant parallel manipulators. IEEE Transactions on Robotics. 2011;27:1137-43.
[20] Sarosi J. New approximation algorithm for the force of Fluidic Muscles. 7th IEEE International Symposium on Applied Computational Intelligence and Informatics. Timisoara2012. p. 229-33.
[21] Siegler S, Chen J, Schneck CD. The three-dimensional kinematics and flexibility characteristics of the human ankle and subtalar joints—Part I: kinematics. J Biomech Eng. 1988;110:364-73.
[22] Parenteau CS, Viano DC, Petit PY. Biomechanical properties of human cadaveric ankle-subtalar joints in quasi-static loading. J Biomech Eng. 1998;120:105-11.
[23] Jamwal PK, Hussain S, Xie SQ. Three-Stage Design Analysis and Multicriteria Optimization of a Parallel Ankle Rehabilitation Robot Using Genetic Algorithm. IEEE Transactions on Automation Science and Engineering. 2015;12:1433-46.
[24] Jamwal PK, Xie S, Aw KC. Kinematic design optimization of a parallel ankle rehabilitation robot using modified genetic algorithm. Robotics & Autonomous Systems. 2009;57:1018-27.
[25] Tsoi YH. Modelling and adaptive interaction control of a parallel robot for ankle rehabilitation [PHD thesis]: The University of Auckland; 2011.
[26] Qian Z, Bi Z. Recent Development of Rehabilitation Robots. Advances in Mechanical Engineering. 2014.
[27] Yoon J, Ryu J. A novel reconfigurable ankle/foot rehabilitation robot. IEEE International Conference on Robotics and Automation. Barcelona, Spain2005. p. 2290-5.